***Title:***

# Simple noise reduction for diffusion weighted images

***Author Names:***

Yuto Konishi,[1] Yuki Kanazawa,[2] Takatoshi Usuda,[1] Yuki Matsumoto,[1]
Hiroaki Hayashi,[2] Tsuyoshi Matsuda,[3] Junji Ueno,[2] and Masafumi Harada[4]

***Author Affiliations:***

[1] School of Health Sciences, Tokushima University
3-18-15, Kuramoto-Cho, Toksuhima City, Tokushima, 770-8503, Japan
[2] Institute of Biomedical Sciences, Tokushima University Graduate School
3-18-15, Kuramoto-Cho, Toksuhima City, Tokushima, 770-8503, Japan
[3] MR Applications and Workflow Asia Pacific GE Healthcare Japan Corporation
4-7-127, Asahigaoka, Hino-city, Tokyo, 191-8503, Japan
[4] Department of Radiology and Radiation Oncology, Institute of Biomedical Sciences, Tokushima University Graduate School
3-18-15, Kuramoto-Cho, Tokushima City, Tokushima 770-8509, Japan

***Corresponding Author*** and ***Reprint Info:***

Yuki Kanazawa, PhD
Institute of Biomedical Sciences, Tokushima University Graduate School
3-18-15, Kuramoto-Cho, Toksuhima City, Tokushima, 770-8509, Japan
Tel: +81 88 633 9059
Fax: +81 88 633 9059
E-mail: yk@tokushima-u.ac.jp

***A concise and informative title:***

Simple noise reduction for DWI

**s**

**Abstract**

Our purpose in this study was to reduce the noise in order to improve the SNR of Dw images with high b-value by using two correction schemes. This study was performed with use of phantoms made from water and sucrose at different concentrations, which were 10, 30, and 50 weight percent (wt%). In noise reduction for Dw imaging of the phantoms, we compared two correction schemes that are based on the Rician distribution and the Gaussian distribution. The highest error values for each concentration with use of the Rician distribution scheme were 7.3% for 10 wt%, 2.4% for 30 wt%, and 0.1% for 50 wt%. The highest error values for each concentration with use of the Gaussian distribution scheme were 20.3% for 10 wt%, 11.6% for 30 wt%, and 3.4% for 50 wt%. In Dw imaging, the noise reduction makes it possible to apply the correction scheme of Rician distribution.

**key words:** magnetic resonance imaging (MRI); diffusion weighted imaging; probability distribution function (PDF); Rician distribution; Gaussian distribution; correction scheme

## 1 Introduction

Diffusion weighted (Dw) magnetic resonance (MR) imaging has recently become a useful technique for evaluating various diseases, e.g., acute cerebral infractions and tumors [1]. Dw MR imaging is a method for imaging of incoherent motions. In Dw MR imaging, the *b*-value represents the intensity of the gradient magnetic field. Dw images with high *b*-value are influenced less by perfusion but more by diffusion. It is becoming more important to apply an analysis method with high *b*-value, e.g., q-space -analyzed Dw MRI [2], diffusional kurtosis imaging [3], and modified tri-exponential analysis of intravoxel incoherent motion [4]. The signal intensity (SI) of the Dw image is decreased by echo time (TE) prolongation, and this leads to a low signal-to-noise ratio (SNR) [5]. Additionally, it has been reported that a low SNR influences the determination of the apparent diffusion coefficients (ADCs) [6], or leads to failure in measuring diffusion anisotropy [7].

MR images are commonly presented as magnitude images. The magnitude images are made by reconstruction of real images and imaginary images [8]. These images are acquired by a quadrature detector system; they are influenced by the

statistical image noise. Before reconstruction, the noise from these images has characteristics of a Gaussian distribution. On the other hand, the magnitude image has not only the characteristics of a Gaussian distribution, but also these of a Rician distribution [9]. The characteristics of a Rician distribution indicate that the magnitude image does not have a negative value. This distribution has characteristics that differ from those of the Gaussian distribution. Many reports referred to the Rician distribution, e.g., $R_2{}^*$estimation of the liver [10], and determination of the optimal *b*-value in diffusion tensor imaging [11]. Thus, it is important with MR imaging to assess the relationship between the signal values and the Rician distribution.

Therefore, the signal correction in high *b*-value images is expected to yield improved images, i.e., noise reduction images, as a consequence of application of the Rician distribution. We became interested in correction schemes from past reports of Henkelman [8] and/or Gudbjartsson and Patz [9], because it makes it possible to correct the signal when the SNR is low. Previous articles [6] did not describe high *b*-value Dw noise reduction with use of these schemes. Our purpose in this our study was to reduce the noise in order to improve the SNR of Dw images with a high *b*-value by using two

correction schemes based on the probability distributions.

## 2 Materials and methods

### 2.1 Magnitude image of MR imaging

MR images consist of reconstruction of real images and imaginary images. The SI from the pixel $(x, y)$ in a complex MR image was described by Henkelman [8]:

$$S_{(x,y)} = A_{(x,y)} + N_{R(x,y)} + iN_{I(x,y)}, \quad (1)$$

where $S_{(x,y)}$ is the measured SI, $A_{(x,y)}$ is the true SI of the pixel $(x, y)$, and $N_{R(x,y)}$and $N_{i(x,y)}$ are the noise components. The magnitude of the SI, $M_{(x,y)}$, is described as follows:

$$M_{(x,y)} = \left|S_{(x,y)}\right| = [(A_{(x,y)} + N_{R(x,y)})^2 + N^2{}_{I(x,y)}]^{1/2}. \quad (2)$$

### 2.2 Probability distribution

The probability density function (PDF) for the Gaussian distribution for the measured magnitude SI $M$ is given by

$$P(M) = \frac{1}{\sqrt{2\pi\sigma^2}} \exp(-\frac{(M-\mu)^2}{2\sigma^2}), \quad (3)$$

where $\mu$ is mean, and $\sigma$ is the standard deviation (SD).

The PDF for the Rician distribution for $M$ is given in reference [9]:

$$P_M(M) = \frac{M}{\sigma^2}\exp(-\frac{(M^2+A^2)}{2\sigma^2})I_0(\frac{A \cdot M}{\sigma^2}) , \quad (4)$$

where $A$ is the true SI, and $I_0$ is the modified zeroth-order Bessel function. The characteristics of the Rician distribution differ from those of the Gaussian distribution when the SNR is low. However, when the SNR is high, it is approximately equal to the Gaussian distribution [9]. When the SNR is high, the Rician distribution is approximated by Eq. (5) [9]:

$$P_M(M) \approx \frac{1}{\sqrt{2\pi\sigma^2}}\exp(-\frac{(M-\sqrt{A^2+\sigma^2})^2}{2\sigma^2}). \quad (5)$$

The noise distribution of a magnitude image at a high SNR can be regarded as the Gaussian distribution with mean $\sqrt{A^2+\sigma^2}$ and variance $\sigma^2$, as determined by Eq. (5). The postprocessing correction scheme introduced by Gudbjartson and Patz suggested that it was possible to reduce noise by using the following relationship [9]:

$$\tilde{A}_1 = \sqrt{|M^2-\sigma^2|} , \quad (6)$$

where $\tilde{A}_1$ is the corrected SI. We used Eq. (6) as behaving the correction scheme based on the Rician distribution.

There is a relationship, $\overline{M^2} = A^2 + 2\sigma^2$, between the mean of the measured SI

and the true SI in the magnitude image [8]. Then, the following correction scheme has been established [9]:

$$\tilde{A}_2 = \sqrt{|M^2 - 2\sigma^2|}, \quad (7)$$

where $\tilde{A}_2$ is the corrected SI. We established Eq. (7) as behaving the correction scheme based on the Gaussian distribution.

### 2.3 MR imaging

On a 1.5T MRI system (Signa HDxt, GE Healthcare, Waukesha, WI, USA), Dw imaging of a phantom was performed with single-shot spin-echo echo planar imaging (SS-SE-EPI). To acquire Dw images of ADC, we made phantoms by using sucrose solutions of different concentrations (10, 30, and 50 wt%) [12]. Each phantom was placed in the center of a standard head coil. The imaging parameters of Dw imaging were repetition time, 5000 ms; TE, 129.2 ms; slice thickness, 10 mm; field of view, 12.8 × 6.4 $cm^2$; and *b*-values, 0, 20, 200, 500, 1000, 2000, 3000, 4000, 4500, 5000, 5500, 6000, 6500, and 7000 $s/mm^2$.

### 2.4 Data analysis

A typical example of the region-of-interest (ROI) setting is shown in Fig. 1. We

measured SIs at the ROI (for the size of 15 × 15 pixels). Then we measured the mean SI $M$ and SD $\sigma$ in the ROI. Next, we calculated each PDF by using an in-house program from MATLAB (MathWorks, Natick, MA, USA). We derived the most frequent value $\alpha$ from a peak value of fitting each PDF. Furthermore, we calculated each corrected SI ($\tilde{A}_1$ and $\tilde{A}_2$) from Eq. (6) and Eq. (7).

To assess the results of correcting the measured SI in Dw imaging, we evaluated error values in each $b$-value Dw image. The error value is defined by Eq. (8):

$$error\ [\%] = \frac{|\alpha - \tilde{A}|}{\alpha} \times 100. \quad (8)$$

When the error was small, we regarded the effect as accurate performance.

## 3 Results

Table 1 shows the relationship between $b$-values and several signal-to-standard deviation ratios for each phantom.

Figure 2 shows the Dw images (a, b, and c) of each sucrose phantom. Each SI for a Dw image was shown to decrease at the higher $b$-values. Some white arrows show Nyquist N/2 ghosting artifacts.

Figure 3 shows the PDFs from the Rician distribution (a, b, and c). The PDFs shifted to low intensity, and the variances were low at higher *b*-values.

Figure 4 shows the error between the corrected SI and the most frequent value of SI. The highest error values for each phantom concentration (10, 30, and 50 wt%), in correction by the correction scheme based on the Rician distribution, were 7.3, 2.4, and 0.1%, respectively. The highest error values for each of the three phantom concentrations, in correction by the correction scheme based on the Gaussian distribution, were 20.3, 11.6, and 3.4%, respectively. When $\alpha/\sigma$ was lower than 1.4, the error value was determined by application of the correction scheme based on the Rician distribution, which was higher than 5.0%. In addition, when $\alpha/\sigma$ was lower than 3.0, the error values were determined by application of the correction scheme based on the Gaussian distribution, then were higher than 5.0% (Table 1 and Fig.4).

## 4 Discussion

In our study, to investigate the usefulness of two correction schemes, i.e., based on the Rician distribution or the Gaussian distribution, we compared the most frequent values

of SI and the corrected SIs. When the *b*-value was low, i.e., the SNR showed a high enough value, the errors were almost zero% regardless of the correction methods used. These results would indicate that the Rician distribution is able to approximate the Gaussian distribution. However, if the *b*-value was high, i.e., the SNR showed a low value, the error values of the corrected SI by use of the Gaussian distribution scheme showed values higher than 5%. Nevertheless, the error values of the corrected SI by the Rician distribution were constantly lower than 5% except in a Dw image of 5500 s/mm$^2$ *b*-value with a 10 wt% sucrose phantom. Therefore, for correction of the SI of Dw images, it is possible to apply the Rician distribution correction scheme.

The correction scheme based on the Gaussian distribution was derived from the relationship between the most frequent value of SI and the measured SI by Henkelman [8]. This correction scheme involves fitting of a monoexponential function; hence it is thought to be impossible to use it in unsuitable conditions, e.g., multi-exponential characteristics [9]. In our study, we defined the SNR as $\alpha/\sigma$. Although we applied this correction scheme to the measured SI of Dw images, we could not correct it when the SNR values were lower than 3.0. This result would show that the decay of SI did not

follow a monoexponential function when the SNR was very low.

Dietrich et al. reported that the correction scheme based on the Rician distribution shows the advantages of easy calculation and ability to handle averaged-magnitude images [6]. However, this scheme is not recommended when the SNR is very low [6]. In our study, we could not precisely correct the SI, i.e., the error value became larger than ±5%, for a Dw image of 5500 s/mm$^2$ *b*-value with a 10 wt% sucrose phantom. The SNR value for this image was 1.4, which was the smallest value in this experiment. Consequently, we were not able to correct the measured SI by the Rician distribution. It may be necessary to acquire Dw images with lower SNR values than those used in our study.

There were several limitations to our study. First, we performed experiments by using the SS-SE-EPI sequence. Here, the images which we used appeared as the Nyquist N/2 ghosting artifacts of low *b*-value in the phase encoding direction (Fig. 2, white arrows). Because the phantom size was small, it was not affected by the Nyquist N/2 ghosting artifacts; if a subject size is larger, we would have to be careful. The SS-SE-EPI sequence, moreover, has often been selected for Dw MR imaging and reduces

1 the imaging time and motion artifacts [13]. However, this sequence is sensitive to some
2 artifacts such as image ghosts, which are caused by gradient pulse switching delays and
3 eddy currents [14]. The Dw images in our study had much noise, and it was difficult to
4 distinguish between the phantom signal and noise in a high *b*-value image. Although we
5 attempted to correct the SI, we should consider other factors for improving Dw images;
6 it may be necessary use with other pulse sequences, e.g., dual-spin-echo EPI [15] or
7 PROPELLER (Periodically Rotated Overlapping ParallEL Lines with Enhanced
8 Reconstruction) [16]. Second, in Dw MR imaging of human subjects, the SI follows a
9 non-monoexponential decay. Kristoffersen reported that the statistical models of signal
10 decay of the human brain are non-monoexponential models with several parameters
11 [17]. It would be difficult to define the noise level because the SI decreases with the
12 non-monoexponential model. The phantoms consisting of sucrose in our experiments
13 tended to follow the monoexponential decay of SI, and they were intended for use in
14 evaluation of the potential of each correction scheme. However, we did not consider the
15 non-monoexponential decay seen in the human body. Besides, it was not obvious
16 whether the correction schemes we used are useful in non-monoexponential decays of

the SI. It may be necessary to apply a non-monoexponential phantom model composed of multiple materials like those in a clinical environment. Third, there was an opinion that our approximation of the Rician distribution was inaccurate [18]. Andersen showed another approximation, which is also accurate. However, we applied the approximation proposed by Gudbjartsson because the equation was simple and fitted the Rician distribution properly. It may be necessary to compare the two approximations.

## 5 Conclusion

We tried to improve the SNR of Dw images with high *b*-value by using two existing correction schemes, i.e., the Gaussian PDF and the Rician PDF. In our phantoms experiment, we found that the correction scheme based on the Rician PDF is better than that based on the Gaussian PDF at a low SNR. In Dw imaging, the correction of the SI makes it possible to apply a correction scheme based on the Rician distribution.

## Conflict of interest

An author, Tsuyoshi Matsuda, is an employee of the GE Healthcare Corporation, Tokyo, Japan. All remaining authors have declared no conflicts of interest.

## References


1. Le Bihan D, Breton E, Lallemand D, Grenier P, Cabanis E, Laval Jeantet M. MR Imaging of Intravoxel Incoherent Motions: application to Diffusion and Perfusion in Neurologic Disorders. Radiology. 1986;161:401-407.

2. Assaf Y, Ben-Bashat D, Chapman J, Peled S, Biton IE, et al. High *b*-value *q*-Space Analyzed Diffusion-Weighted MRI: Application to Multiple Sclerosis. Magn Reson Med. 2002;47:115-126.

3. Fieremans Els, Jensen JH, Helpern JA. White matter characterization with diffusional kurtosis imaging. NeuroImage. 2011;58:177-188.

4. Ohno N, Miyati T, Kobayashi S, Gabata T. Modified Triexponential Analysis of Intravoxel Incoherent Motion for Brain Perfusion and Diffusion. J Magn Reson Imaging. 2015; e-pub. doi: 10.1002/jmri.25048.

5. Gatidis S, Schmidt H, Martiosian P, Nikolaou K, Schwenzer NF . Apparent Diffusion Coefficient-Dependent Voxelwise Computed Diffusion-Weighted Imaging : An Approach for Improving SNR and Reducing $T_2$ Shine-Through Effects. J Magn Reson Imaging. 2015; e-pub. doi: 10.1002/jmri.25044

6. Dietrich O, Heiland S, Sartor K. Noise Correction for the Exact Determination of Apparent Diffusion Coefficients at Low SNR. Magn Reson Med. 2001;45:448-453.

7. Bastin ME, Armitage PA, Marshall I. Atheoretical study of the effect of experimental noise on the measurement of anisotropy in diffusion imaging. Magn Reson Imaging 1998;16:773-785.

8. Henkelman RM. Measurement of signal intensities in the presence of noise MR images. Med phys. 1985;12(2):232-233.

9. Gudbjartsson H, Patz S. The Rician Distribution of Noisy MRI Data. Magn Reson Med.1995;34(6):910-914.

10. Yokoo T, Yuan Q, Senegas J, Wiethoff AJ, Pedrosa I. Quantitative $R_2^*$ MRI of the Liver With Rician Noise Models for Evaluation of Hepatic Iron Overload : Simulation, Phantom, and Early Clinical Expertence. J Magn Reson Imaging. 2015; e-pub. doi: 10.1002/jmri.24948

11. Taylor PA, Biwal B. Geometric analysis of the *b*-dependent effects of Rician signal noise on diffusion tensor imaging estimates and determining an optimal *b* value.

Magn Reson Imaging. 2011;29:777-788.

12. Tamura T, Usui S, Akiyama S. Investigation of a phantom for Diffusion Weighted Imaging That Contorolled the Apparent Diffusion Coefficient Using Gelatin and Sucrose. Nihon houshasen Gijutu Gakkai Zasshi. 2009;65(11):1485-1493.

13. Robert I, DeLaPaz, MD. Echo planner imaging. RadioGraphics. 1994;14(5): 1045-1058.

14. Wilm BJ, Nagy Z, Barnet C, Vannesjo SJ, Kasper L, Haeberlin M, et al. Diffusion MRI with Concurrent Magnetic Field Monitoring. Magn Reson Med. 2015;74:925-933.

15. Reese TG, Heid O, Weisskoff RM, Wedeen VJ. Reduction of Eddy-Current-Induced Distortion in Diffusion MRI Using a Twice-Refocused Spin Echo. Magn Reson Med. 2003;49:177-182.

16. Pipe JG, Farthing VG, Forbes KP. Multishot Diffusion-Weighted FSE Using PROPELLER MRI. Magn Reson Med. 2002;47:42-52.

17. Kristoffersen A. Statistical Assessment of Non-Gaussian Diffusion Models. Magn Reson Med. 2011;66:1639-1648.

18. Andersen AH. On the Rician Distribution of Noisy MRI Data. [Letter to the Editor]. Magn Reson Med. 1996;36:331-333.

**Figure legends**

**Figure 1** ROI setting for Dw images. The ROI size of all analyzed images was fixed at 15 × 15 pixels (outlined by the black square box).

**Figure 2** The Dw MR images of each *b*-value from 0-7000 s/mm$^2$ are shown in the left-to-right direction. In the top-to-bottom direction, different sucrose concentrations were shown. **a** Sucrose concentration 10 wt%, **b** Sucrose concentration 30 wt%, **c** Sucrose concentration 50 wt%. White arrows show Nyquist N/2 ghosting artifacts.

**Figure 3** ~~The p~~ Probability distributions of measured SI for Dw images of each sucrose phantom. Here, the probability distributions are shown in specific data because we focused on the points to distinguish between signal and noise. **a.** Sucrose concentration 10 wt% phantom; *b*-values = 2000, 3000, 4000, 4500 s/mm$^2$. **b.** Sucrose concentration 30 wt% phantom; *b*-values = 4000, 4500, 5000, 5500 s/mm$^2$. **c.** Sucrose

concentration 50 wt% phantom; *b*-values = 5500, 6000, 6500, 7000 s/mm$^2$.

**Figure 4** Error values between correction SI and most frequent value of SI. **a** Sucrose concentration 10 wt%, **b** Sucrose concentration 30 wt%, **c** Sucrose concentration 50 wt%. The dashed lines in these figures represent error values of ± 5%. When the error values were higher than these lines, the SI correction was considered a failure.

**Table 1** Relationship between *b*-value and several signal-to-standard deviation ratios for each phantom.

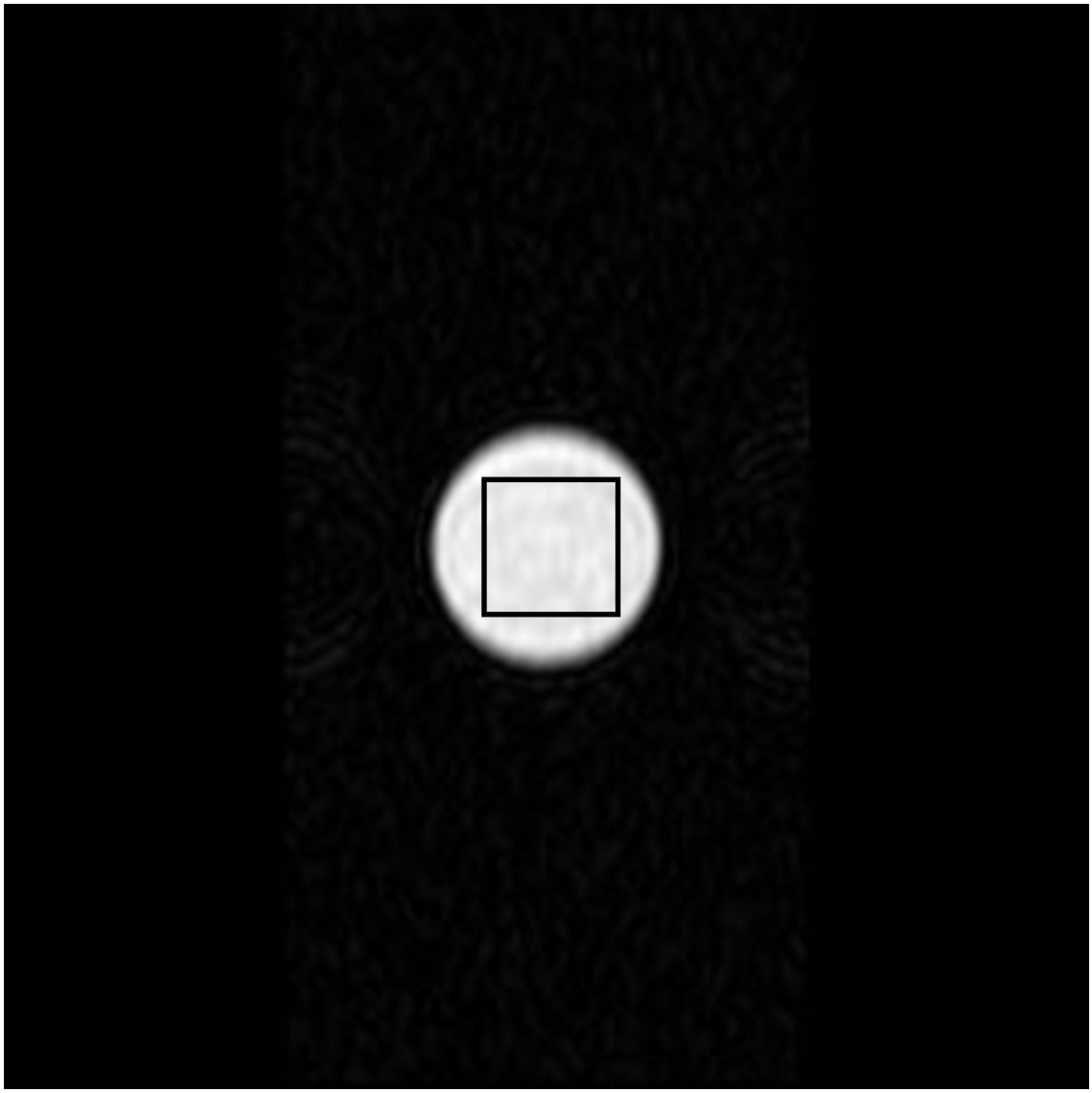

**Fig. 1**

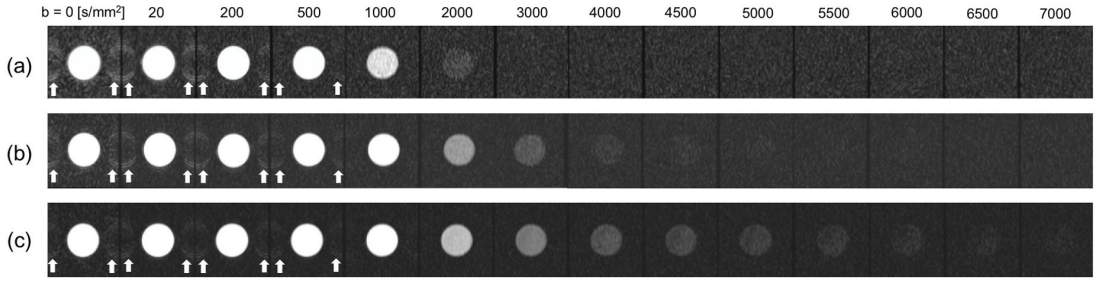
b = 0 [s/mm²]
20
200
500
1000
2000
3000
4000
4500
5000
5500
6000
6500
7000
(a)
(b)
(c)

1

2 **Fig. 2**

3

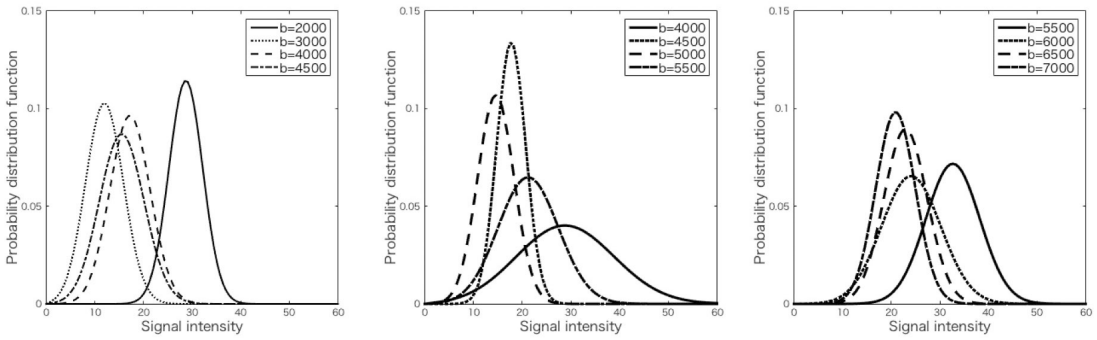
Probability distribution function
Signal intensity
b=2000
b=3000
b=4000
b=4500
b=4000
b=4500
b=5000
b=5500
b=5500
b=6000
b=6500
b=7000
(a)
(b)
(c)

1

2 **Fig. 3**

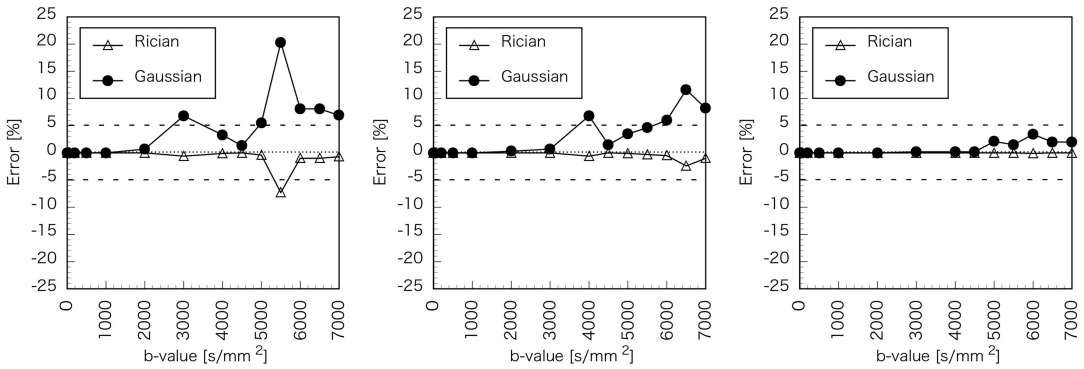


1

2 **Fig. 4**

3

**Table 1** Relationship between *b*-value and several signal-to-standard deviation ratios for each phantom.

| *b*-values [s/mm$^2$] | 10 wt% sucrose | | | 30 wt% sucrose | | | 50 wt% sucrose | | |
|---|---|---|---|---|---|---|---|---|---|
| | $\alpha/\sigma$ | $\widetilde{A_1}/\sigma$ | $\widetilde{A_2}/\sigma$ | $\alpha/\sigma$ | $\widetilde{A_1}/\sigma$ | $\widetilde{A_2}/\sigma$ | $\alpha/\sigma$ | $\widetilde{A_1}/\sigma$ | $\widetilde{A_2}/\sigma$ |
| 0 | 51.5 | 51.5 | 51.4 | 58.0 | 58.0 | 58.0 | 87.5 | 87.5 | 87.5 |
| 20 | 94.4 | 94.4 | 94.4 | 79.0 | 79.0 | 79.0 | 139.4 | 139.4 | 139.4 |
| 200 | 76.7 | 76.7 | 76.7 | 82.6 | 82.6 | 82.6 | 100.9 | 100.9 | 100.9 |
| 500 | 60.2 | 60.2 | 60.2 | 73.1 | 73.1 | 73.1 | 87.7 | 87.7 | 87.7 |
| 1000 | 34.1 | 34.1 | 34 | 48.8 | 48.8 | 48.8 | 94.6 | 94.6 | 94.6 |
| 2000 | 8.1 | 8.1 | 8.1 | 14.0 | 14.0 | 14.0 | 34.5 | 34.5 | 34.5 |
| 3000 | 2.6 | 2.6 | 2.5 | 8.8 | 8.8 | 8.7 | 15.4 | 15.4 | 15.3 |
| 4000 | 3.8 | 3.8 | 3.7 | 2.6 | 2.6 | 2.4 | 16.7 | 16.7 | 16.7 |
| 4500 | 6.2 | 6.2 | 6.1 | 5.8 | 5.8 | 5.8 | 17.5 | 17.5 | 17.5 |
| 5000 | 3.0 | 3.0 | 2.8 | 3.7 | 3.7 | 3.6 | 5.0 | 5.0 | 4.9 |
| 5500 | 1.4 | 1.5 | 1.1 | 3.2 | 3.2 | 3.1 | 5.8 | 5.8 | 5.7 |
| 6000 | 2.4 | 2.4 | 2.2 | 2.8 | 2.8 | 2.6 | 3.8 | 3.8 | 3.6 |
| 6500 | 2.4 | 2.4 | 2.2 | 1.9 | 2.0 | 1.7 | 5.0 | 5.0 | 4.9 |
| 7000 | 2.6 | 2.6 | 2.4 | 2.4 | 2.4 | 2.2 | 5.0 | 5.0 | 4.9 |

$\alpha$, the most frequent value of signal value on fitting probably density function; $\widetilde{A_1}$, the corrected signal value derived from the Rician distribution scheme; $\widetilde{A_2}$, the corrected signal value derived from the Gaussian distribution scheme; $\sigma$, standard deviation.